

The temperature and excitation power density dependent photoluminescence study of Ga-doped ZnO thin films

S. KAYRAL, R. TÜLEK, S. GÖKDEN*, A. TEKE

Department of Physics, Faculty of Science and Letter, Balıkesir University, Çağış Kampüsü, 10145 Balıkesir, Turkey

Temperature and excitation power density dependent photoluminescence (PL) studies were performed on Ga-doped ZnO (GZO) thin films grown on a-(11̄20) and c-(0001) sapphire substrates by Molecular Beam Epitaxy (MBE). The observed PL spectra are dominated by excitonic as well as defect related transitions. The origins of the emission bands were determined by applying the Gaussian fit to 10K PL spectra and discussed and compared with those available in literature. The shape of the temperature dependence of the PL spectra did show any discernable dependence on the substrate orientation used. The peak energies of excitonic transitions redshifted with increasing temperature with a total shift of about 70 meV (from 10K to 300 K). From the temperature activation energies of 6 and 40 meV were obtained from a bi-exponential empirical equation fitting. The excitation power density dependence of total integrated PL intensities and the ratio of peak intensities of the excitonic transition to yellow luminescence revealed that they follow a power law in the form of $I_T \text{ or } I_{ex}/I_{YL} \propto P_E^k$, where P_E is the excitation power density and k is the power factor.

(Received October 19, 2021; accepted October 5, 2022)

Keywords: Ga-doped ZnO (GZO), Photoluminescence (PL), Exitonic transitions, Optical properties

1. Introduction

Zinc oxide (ZnO) as a direct wide band gap semiconductor is one of the promising materials in optoelectronics especially in devices utilizing excitonic transitions and has been the subject of investigations panning on many years [1-5]. For thermally stable transparent electrodes such as that used in solar cell applications, ZnO is frequently doped with group III and VII elements [6, 7]. Of these, Ga⁺³ ions can substitute at Zn²⁺ lattice sites without significant lattice mismatch and deformation [8, 9]. It has been reported that Ga doped ZnO (GZO) has high carrier density and electrical conductivity [10]. Gupta et al. [11] reported defect-induced photoluminescence behavior of GZO thin films grown on silicon substrate with varying doping (Ga) concentrations. The PL spectra showed near-band-edge (NBE) emissions including free excitons (FX), donor-bound excitons (DX), acceptor-bound excitons (AX) and their phonon replicas along with broad violet, blue, green, yellow, and red emission bands. It has been observed that the blue-violet emission band increases with increasing Ga density. The transitions observed in the visible band of the spectrum were attributed to natural point and/or complex defects [11]. In photoluminescence study of GZO thin films on grown pure silica glass substrate, various intrinsic and extrinsic emission bands were observed at room temperature [12]. Z. Yang et al. studied Ga-related photoluminescence lines in Ga-doped ZnO grown on r-plane sapphire substrates using plasma-assisted molecular-beam epitaxy (MBE). From the excitation-power dependence of the luminescence, it has been shown that the donor-acceptor transition energy clearly blueshifts with excitation power [13]. In another study, Hiroyuki Kato et al. studied Gallium-doped ZnO

epitaxial layers grown on a-plane sapphire substrates by molecular beam epitaxy (MBE) and it has been shown that the photoluminescence (PL) spectra of Ga-doped ZnO were dominated by an emission at 3.362 eV which can be assigned to emission related to excitons bound to Ga-related neutral donors [14]. Ray-Hua Horng et al. also investigated the effects of Ga concentration on PL properties of GZO thin films grown on (0001) sapphire substrates by using a MOCVD and it has been shown that a blueshift in bandgap peaks was occurred and the intensity of the bandgap to broad band luminescence peaks was increased [15].

Because GZO thin films are mostly used as semi-transparent electrodes in back illuminated solar cells it is crucial to transmit solar radiation to the active region for absorption. Along with high electrical conductivity requirements, identification of the optical quality and defect centers in GZO thin films is considered an important issue to improve solar cells performance. Therefore, optical properties of GZO layers grown by molecular beam epitaxy (MBE) on two different sapphire substrates c-(0001), a-(11̄20) were studied in detail in this study using temperature (10K-300K) and excitation power density (2.6-330 mW/cm²) dependent photoluminescence experiments.

2. Results and discussions

The samples coded as 651 and 753 were grown on c- and a- sapphire substrates, respectively, by MBE. For these two samples, the growth was initiated with the deposition of a low temperature ZnO (LT-ZnO) layer and followed by high temperature ZnO (HT-ZnO) layer. The growth details are given in Table 1 for samples 651 and 753.

Table 1. The growth conditions and parameters of samples

Sample Code		651	753
Substrate		a- sapphire	c- sapphire
Total Thickness (nm)		300	210
Low Temperature	Substrate temperature (°C)	200	200
	ZnO Temperature (°C)	570	640
	Pressure (Torr)	9.1x10 ⁻⁶	8x10 ⁻⁶
High Temperature	Substrate temperature (°C)	611	550
	ZnO Temperature (°C)	590	590
	Pressure (Torr)	9x10 ⁻⁶	6.2x10 ⁻⁶
Growth Time (min.)		250	120

Temperature and excitation power density dependent photoluminescence measurements were performed on samples placed in a closed-cycle cryostat in the temperature range between 10 to 300K. A 349 nm frequency triple Nd: YLFQ switched pulse laser was used for excitation.

Luminescence was collected with the appropriate lenses and then dispersed with a 500 mm spectrometer using 1200 lines/mm grating. The optical signal was detected with a computer controlled Concentrated Charge Coupled Device (ICCD) camera.

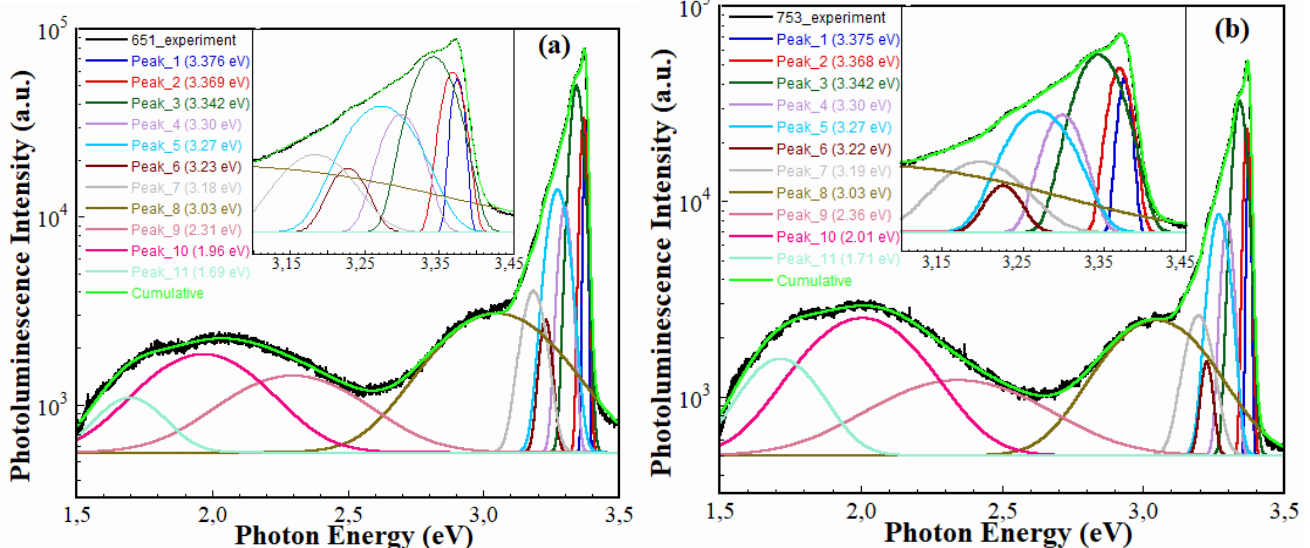


Fig. 1. The applied Gaussian fittings (purple solid lines) on 10K PL spectra for sample (a) 651, (b) 753. Inset shows enlarged part of excitonic transition regions (color online)

Fig. 1 shows 10K PL spectra of samples with applied Gaussian fittings which allows deconvolution of the closely spaced peaks and shoulders that exist in broad spectra as observed in our samples. When ZnO films are intentionally doped with Ga, free exciton transitions are expected to be relatively weak compared to high quality single crystal or undoped ZnO thin films [16, 17]. The peaks that are resolved from fittings were examined and compared with those available in the literature. From these fittings, the peak positions observed as shoulders on high energy side of the main peak were resolved at about 3.376 eV. These peaks

correspond to the A free exciton of ZnO (FXA), which are consistent with values of 3.376-3.378 eV reported for high quality ZnO in the literature [18-22]. The transitions obtained from the Gaussian fitting at the peak energy values of 3.368-3.369 eV are due to the shallow neutral donor bound A free excitons (DBE). These donor-bound exciton peak positions are about 7 meV lower than the A free exciton transition and may represent donor binding energies. Similarly, the transitions deconvolved from the Gaussian fitting at the peak energies of about 3.342-3.343 eV are attributed to the shallow neutral acceptor bound A

free excitons (ABE). These acceptor-bound exciton peak positions are 33 meV lower than the A free exciton and may represent acceptor binding energies. In general, the defect centers and their relative densities in intentionally or unintentionally doped semiconductors may differ in the literature depending on their formation energies as well as their structure (low-dimensional or bulk) and growth methods used [23].

The Fröhlich interactions in polar and wide bandwidth materials such as ZnO are the most prominent exciton-phonon scattering mechanism induced by longitudinal optical phonons (LO) [24]. These strong interactions manifest themselves as phonon replica of main excitonic and/or defect-related transitions in PL spectra. LO phonon energy of ZnO is around 71–73 meV [25]. Accordingly, the peak energy values of 3.299 and 3.228 eV (for the 651 sample) and 3.298 and 3.225 eV (for the 753 sample) derived from the Gaussian fittings are due to 1-LO and 2-LO phonon replicas of the main A free exciton and donor-bound exciton transitions. Because the optical quality of the samples is not as high as that of high-quality bulk samples, LO replicas of the main transitions could not be resolved

separately. Therefore, these peak energies represent the combined phonon replicas of the main transitions. To reiterate, the energy shifts of about 72 meV are consistent with the LO phonon energy of ZnO. It can be argued that there may also be other bound excitonic and/or donor-acceptor pair (DAP) transitions in these spectral regions. Therefore, shoulders and ridges in this spectrally unresolved region may represent a combination of phonon replicas of free and bound excitonic transitions together with DAP and its phonon replicas.

The low energy sides of 10K PL spectra of all samples can be divided into three spectral regions. The blue luminescence observed at about 3.1 eV can be possibly attributed to the defect due to the zinc vacancy (V_{Zn}) [26–30]. The green luminescence observed at about 2.3 eV can be attributed to the defect due to the substitution of oxygen into the zinc site (O_{Zn}) [27, 28, 31–34]. The yellow luminescence observed at about 2.0 eV can be attributed to the defect centers related to zinc and oxygen interstitial complex (Zn_i/O_i) [34, 35], and finally the red luminescence observed at about 1.7 eV may be related to oxygen interstitial (O_i) defect centers [26, 31, 36–38].

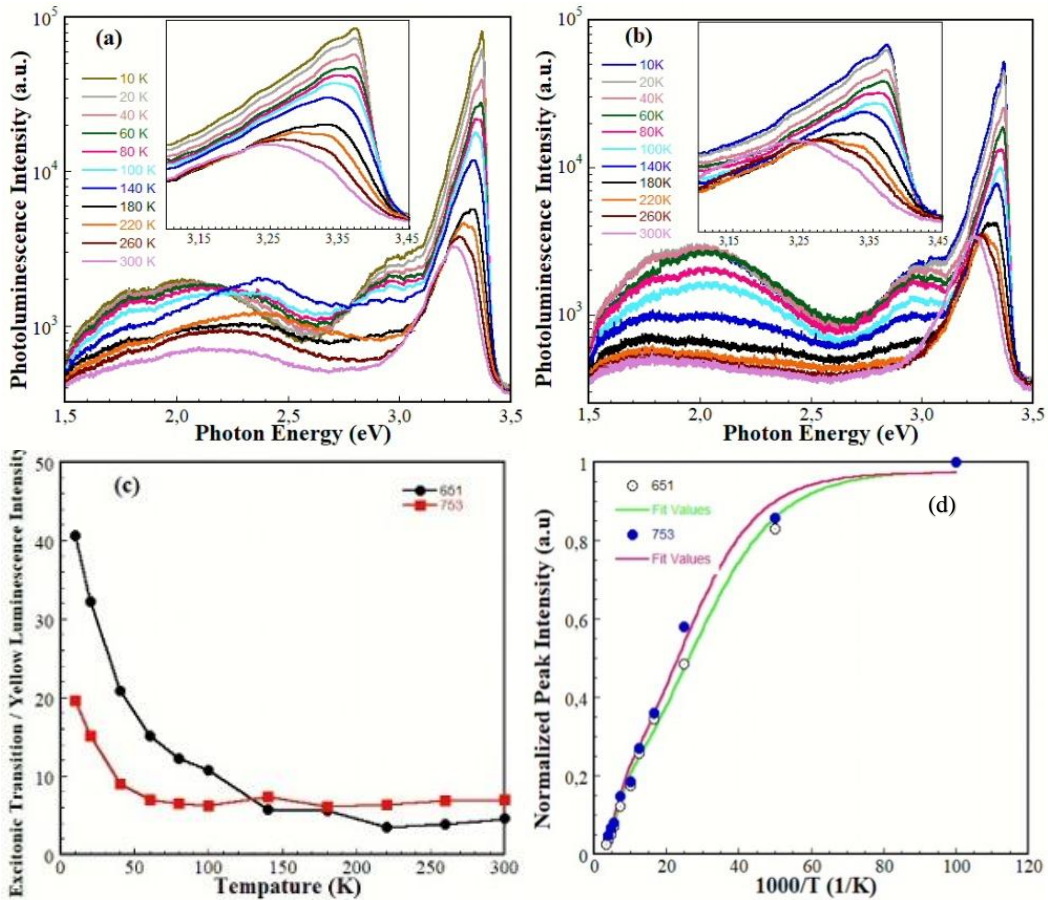


Fig. 2. The PL spectra taken at different temperatures between 10K and 300K for sample (a) 651 and (b) 753. (c) the change of the ratio of main excitonic peak intensity to yellow luminescence intensity with temperature. (d) Normalized peak intensities of excitonic transitions as a function of inverse temperature. Solid lines shows the bi-exponential empirical fittings. Insets show enlarged part of the excitonic regions (color online)

Fig. 2 shows the temperature dependent PL spectra of our samples taken at temperatures between 10K and 300 K.

During these measurements, the excitation power density was kept low to avoid excessive excitation effects. It was

observed that temperature dependent PL spectra for both samples exhibit similar behavior. As the temperature increases, the peak positions of free and bound excitons shift to lower energies by following the band gap narrowing due to the lattice expansion and electron-phonon interactions. Room temperature PL spectra peaked at about 3.27-3.28 eV with a total shift of about 105 meV over the explored temperature range for both samples. It has been commonly observed that the temperature-dependent variation of excitonic peaks is well characterized by the Varshni equation [46] using fitting parameters compatible with the literature [39-41]. On the other hand, the so called blue, green, yellow, and red luminescence peak energies associated with deep level defects centres discussed above do not follow the band gap shrinkage and are virtually temperature independent. It is known that the peak or total PL intensity decreases gradually as the temperature increases, due to the thermal activation of non-radiative centers or the thermal escape of the carriers involved in the emission process. The decrease in PL peak intensity or total integrated intensity, which is generally slower at low temperatures and faster at high temperatures, indicates that more than one non-radiative mechanism is most likely active. For this reason, the bi-exponential approach is used to fit the peak intensities of excitonic transitions as a function of inverse temperature as shown in Fig. 2(d). The total decrease in PL intensity of samples 651 and 753 between 10K and 300K is approximately 40, 25-fold, respectively. The empirical equation with two thermal activations has been found to be very compatible with experimental results. The low (E_{low}) and high (E_{high}) temperature activation energies obtained from the best fitting are in the range of 6 and 40 meV, respectively. The former can be attributed to the temperature-dependent capture cross section of the carriers at the recombination centers, while the latter corresponds to the average thermal energy required for dissociation of excitons. [42]. As seen in Fig. 2, the intensities of the deep level defect related transitions also decrease, albeit at different rates, as the temperature increases. Among them the blue luminescence observed at a peak energy of about 3.05 eV decreases gradually with increasing temperature and almost vanishes

at room temperature for all samples. Similarly, the intensities of the so-called green, yellow, and red luminescence decrease, at different rates, as the temperature increases. For sample 651, the temperature variation of the peak intensities in this spectral region differs slightly from the other sample. It is seen that the intensities of yellow and red luminescence are higher compared to that of green luminescence at low temperatures. When the temperature rises above 100K, the intensity of the green luminescence becomes higher than the yellow and red luminescence peaks. For samples 753, the yellow and red luminescence peak intensities decrease steadily as the temperature increases.

Fig. 2(c) shows the change in the ratio of main excitonic peak intensity to yellow luminescence intensity as a function of temperature. In general, this ratio decreases much faster in the 10K-100K temperature range compared to the temperature region greater than 100K. For sample 651, this ratio is about 41 at 10K, then decreases rapidly to 11 at 100K. Above this temperature it decreases at a slower rate and reaches to 5 at room temperature. There is an 8-fold change in the ratio of the peak intensity of the excitonic transition to the yellow luminescence peak intensity in the temperature range of interest. This ratio at 10K PL spectra is approximately 20 for sample 753. Then, it decreases to 7 at room temperature with approximately 3-fold change in total.

As seen in Fig. 2(d), PL peak intensities decrease at different rates as the temperature increases. The observed decrease in PL intensities between 10K and 300K in samples coded 651 and 753 is approximately 40 and 25 times, respectively. As can be seen in the figure, it is seen that the empirical equation with two thermal activations is in good agreement with the experimental results. The obtained low temperature activation energies in the range of about 6-7 meV can be attributed to the temperature dependent capture cross section of the carriers in the recombination centers, while the high temperature activation energies in the range of 30-45 meV can correspond to the thermal dissociation energy required for the nonradiative recombination of electrons from the excited state to the ground state.

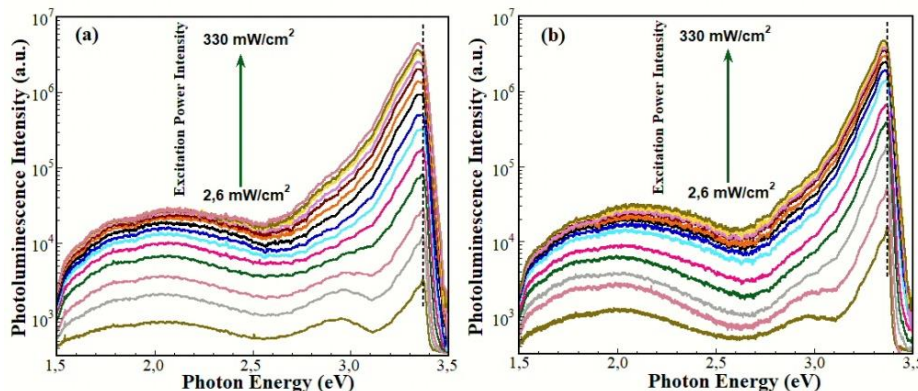


Fig. 3. The 10 K PL spectra taken at various excitation power densities in the range of 2.6-330 mW/cm² for sample; (a) 651 and (b) 753. The dashed vertical lines are placed to help track the change in the peak energy positions (color online)

Fig. 3 shows the PL spectra for both samples taken at 10K for various excitation power densities between 2.6 and

330 mW/cm². As seen in the figure, as the excitation power density increases, the most obvious change in the PL spectra

is the gradual broadening of the linewidths due to the increase in exciton-phonon interactions. The highest intensity peak shifts to lower energy as excitation power density increases and reaches to about 3.35 eV for both samples. This may be due to change in the relative

intensities of FXA, DBE and ABE transitions. Another reason for this shift can be the strong exciton-phonon interactions that is responsible for the observed broadening in the spectra.

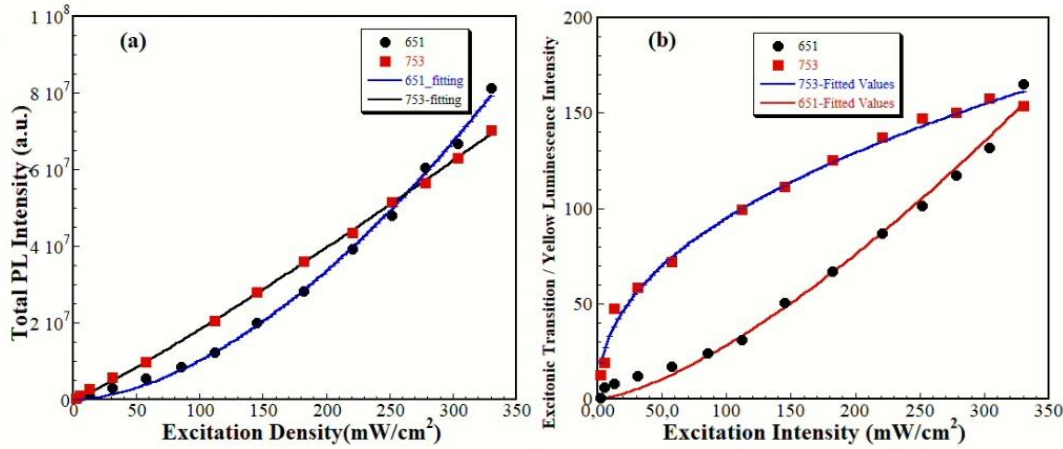


Fig. 4. (a) The variation of the total integrated PL intensity (I_T) as a function of excitation power intensity. (b) The ratio of the highest peak intensity of the excitonic transition (I_{ex}) to the peak intensity of the deep level defect transition (I_{ex}/I_{YL}) (yellow luminescence) as a function excitation power density. The solid lines show the best fits done by a power law in the form of $I_T \propto P_E^k$ or $I_{ex}/I_{YL} \propto P_E^k$, where P_E is excitation power density and k is the power factor (color online)

Fig. 4(a) shows the total integrated intensities of the 10K PL spectra and the ratio of peak intensities of the excitonic transition to yellow luminescence as a function of excitation power density. In general, it is observed that the integrated PL intensity (I_T) follows a power law in the form of $I_T \propto P_E^k$, where P_E is excitation power density and k is the power coefficient in the range of $1 < k < 2$. The power factor depends on the presence of recombination channels and defect levels that can be saturated at sufficiently high excitation power densities. The total PL intensity of sample 651 increases much faster with a $k=1.72$ power factor compared to sample 753. The power factor of sample 753 was found to be $k=1.12$. The linear behavior of the total integrated PL intensity with a slope close to unity may indicate that excitonic transitions are dominant. However, our samples show super linear behavior with different power factors. This may be due to presence of strong exciton-LO phonon interactions. Figure 4(b) shows the ratio of the integrated peak intensities of excitonic transitions to yellow luminescence. This ratio increases with the excitation power density at different rates. It increases with the excitation power density with a power factor of $k = 1.43$ and $k = 0.44$ for sample 651 and 753, respectively. Because the power factor of this ratio is related to the saturation of the relevant transition states, a power factor less than unity may indicate a high defect density in the samples.

3. Conclusions and discussions

The temperature and excitation power density dependent photoluminescence (PL) were studied for Ga-doped ZnO (GZO) thin films grown on sapphire substrates

with two different orientations. The PL spectra were taken in the temperature range of 10K to 300K and excitation power density range of 2.6 to 330 mW/cm². These transitions associated with donor/acceptor bound excitons dominated the 10 K PL spectrum. To resolve the peak position of contributing processes, the spectral transitions were deconvolved by applying a Gaussian fitting method to 10 K PL spectra. To determine their origins, these peaks were tracked up to room temperature, and the results are discussed in comparison with literature. For the peak energies of excitonic transitions, approximately 105 meV total redshift was observed. Temperature-induced activation energies of 6 and 40 meV, on average, were obtained for both samples. With an 8-fold change, the sample 651 showed a much faster rate of decrease in the excitonic peak intensity/yellow luminescence intensity ratio than 753. From the dependence of total PL intensity on the excitation power density, it was determined that the total PL intensity of sample 651 increased much faster than that for sample 753 with a power coefficient of approximately 1.72. Similarly, with a 1.43 power coefficient, excitonic transition/yellow integrated peak intensity ratio of sample 651 increased faster than that in sample 753.

Acknowledgments

Authors thank Hadis MORKOC, Ümit ÖZGÜR and Vitaliy Avrutin from Virginia Commonwealth University for providing the samples used in this study and valuable suggestions on manuscript.

References

- [1] Ü. Özgür, Ya. I. Alivov, C. Liu, A. Teke, M. A. Reschchikov, S. Doğan, V. Avrutin, S.-J. Cho, H. Morkoç, *J. Appl. Phys.*, **98**, 041301 (2005).
- [2] K. Y. Cheong, N. Muti, S. R. Manan, *Thin Solid Films* **410**, 142 (2002).
- [3] W. Lin, R. Ma, J. Xue, B. Kang, *Sol. Energy Mater. Sol. Cells* **91**, 1902 (2007).
- [4] H. J. Lim, D. Yong, Y. J. Oha, *Sensor Actuator A* **125**, 405 (2006).
- [5] A. Ghosh, S. Basu, *Mater. Chem. Phys.* **27**, 45 (1991).
- [6] H. P. Tang, L. P. Zhu, H. P. He, Z. Z. Ye, Y. Zhang, M. Zhi, Z. X. Yang, B. H. Zhao, T. X. Li, *J. Phys. D: Appl. Phys.* **39**, 2696 (2006).
- [7] K. Kobayashi, Y. Tomita, Y. Maeda, S. Matsushima, *Electroceramics Jan. VIII* **301**, 185 (2005).
- [8] R. Kumari, A. Sahai, N. Goswami, *Prog. Nat. Sci.* **25**, 300 (2015).
- [9] H. J. Ko, Y. F. Chen, S. K. Hong, H. Wenisch, T. Yao, D. C. Look, *Appl. Phys. Lett.* **77**, 3761 (2000).
- [10] W. Zhu, S. Kitamura, M. Boffelli, E. Marin, E. D. Gaspera, M. Sturaro, A. Martucci, G. Pezzotti, *Chem. Phys.* **18**, 9586 (2016).
- [11] H. Gupta, J. Singh, R. N. Dutt, S. Ojha, S. Kar, R. Kumar, V. R. Reddy F. Singh, *Chem. Phys.* **21**, 15019 (2019).
- [12] M. Pal, S. Bera, H. Khan, S. Jana, *Kenkyu Journal of Nanotechnology & Nanoscience* **1**, 1 (2015).
- [13] Z. Yang, D. C. Look, J. L. Liu, *Appl. Phys. Lett.* **94**, 072101 (2009).
- [14] H. Katoa, M. Sanoa, K. Miyamotoa, T. Yaob, *Journal of Crystal Growth* **237-239**, 538 (2002).
- [15] R. H. Horngac, S. L. Ou, C. Y. Huang, *Thin Solid Films* **605**, 30 (2016).
- [16] A. T. T Pham, H. K. T. Ta, Y. Liu, M. Aminzare, D. P. Wong, T. H. Nguyen, N. K. Pham, T. B. N. Le, T. Seetawan, H. Ju, S. Cho, K. H. Chen, V. C. Tran, T. B. Phan, J. Alloy. Compd. **747**, 156 (2018).
- [17] H. M. Chiu, Y. T. Chang, W. W. Wu, J. M. Wu, *ACS Appl. Mater. Inter.* **6**, 5183 (2014).
- [18] A. Teke, Ü. Özgür, S. Doğan, X. Gu, H. Morkoç, *Phys. Review* **70**, 1 (2004).
- [19] D. C. Reynolds, D. C. Look, B. Jogai, C. W. Litton, G. Cantwell, W. C. Harsch, *Phys. Rev. B* **60**, 2340 (1999).
- [20] D. C. Reynolds, D. C. Look, B. Jogai, T. C. Collins, *Appl. Phys. Lett.* **79**, 3794 (2001).
- [21] S. F. Chichibu, T. Sota, G. Cantwell, D. B. Eason, C. W. Litton, *J. Appl. Phys.* **93**, 756 (2002).
- [22] D. W. Hamby, D. A. Lucca, M. J. Klopfenstein, G. Cantwell, *J. Appl. Phys.* **93**, 3214 (2003).
- [23] Ü. Özgür, Ya. I. Alivov, C. Liu, A. Teke, M. A. Reschchikov, S. Doğan, V. Avrutin, S. J. Cho, H. Morkoç, *J. Appl. Phys.* **98**, 1 (2005).
- [24] S. Dubey, A. Paliwal, S. Ghosh, *Advanced Materials Research* **1141**, 44 (2016).
- [25] H. Morkoç, Ü. Özgür, *Zinc Oxide: Fundamentals, Materials and Device Technology*, Virginia Commonwealth University: Wiley-Vch Verlag GmbH & Co. KGaA, 2008.
- [26] D. Das, P. Mondal, *RSC. Adv.* **4**, 35735 (2014).
- [27] A. B. Djurišić, W. C. H. Choy, V. A. L. Roy, Y. H. Leung, C. Y. Kwong, K. W. Cheah, T. K. Gundu Rao, W. K. Chan, H. Fei Lui, C. Surya, *Adv. Funct. Mater.* **14**, 856 (2004).
- [28] S. K. Mishra, S. Bayan, R. Shankar, P. Chakraborty, R. K. Srivastava, *Sensor. Actuat. A-Phys.* **211**, 8 (2014).
- [29] A. K. Srivastava, J. Kumar, *Sci. Technol. Adv. Mat.* **14**, 1 (2013).
- [30] X. Jian Ping, Shi Shao-Bo, Li Lan, Zhang Xiao-Song, Wang Ya-Xin, Chen Xi-Ming, *Chinese Phys. Lett.* **27**(4), 047803-1 (2010).
- [31] S. Vempati, J. Mitra, P. Dawson, *Nanoscale. Res. Lett.* **7**, 1 (2012).
- [32] B. Lin, Z. Fu, Y. Jia, *Appl. Phys. Lett.* **79**, 943 (2001).
- [33] H. J. Ko, Y. F. Chen, Z. Zhu, T. Hanada, T. Yao, *J. Cryst. Growth* **208**, 389 (1999).
- [34] A. B. Djurišić, Y. H. Leung, *Small*, **2**, 944 (2006).
- [35] A. Janotti, C. G. Van de Walle, *Phys. Rev. B* **76**, 1 (2007).
- [36] M. C. Jun, S. U. Park, J. H. Koh, *Nanoscale Res. Lett.* **7**, 1 (2012).
- [37] K. J. Chen, F. Y. Hung, S. J. Chang, Z. S. Hu, *Appl. Surf. Sci.* **255**, 6308 (2009).
- [38] B. Panigrahy, M. Aslam, D. S. Misra, M. Ghosh, D. Bahadur, *Adv. Funct. Mater.* **20**(7), 1161 (2010).
- [39] H. J. Ko, Y. F. Chen, Z. Zhu, T. Yao, I. Kobayashi, H. Uchiki, *Appl. Phys. Lett.* **76**, 1905 (2000).
- [40] Y. M. Lu, X. P. Li, P. J. Cao, S. C. Su, F. Jia, S. Han, W. J. Liu, D. L. Zhu, X. C. Y. Ma, M. Lu, J. Spectrosc. **2013**, 1 (2013).
- [41] P. A. Rodnyi, I. V. Khodyuk, *Opt. Spectrosc.* **111**, 776 (2011).
- [42] R. Chen, Y. Tay, J. Ye, Y. Zhao, G. Xing, T. Wu, S. Handong, *J. Phys. Chem. C* **114**, 17889 (2010).

*Corresponding author: sozalp@balikesir.edu.tr